Physics Letters B 286 (1992) 403–412
North-Holland

PHYSICS LETTERS B

Measurement of inclusive η production in hadronic decays of the Z^0

L3 Collaboration

O. Adriani [a], M. Aguilar-Benitez [b], S. Ahlen [c], H. Akbari [d], J. Alcaraz [e], A. Aloisio [f], G. Alverson [g], M.G. Alviggi [f], G. Ambrosi [h], Q. An [i], H. Anderhub [j], A.L. Anderson [k], V.P. Andreev [ℓ], T. Angelov [k], L. Antonov [m], D. Antreasyan [n], P. Arce [b], A. Arefiev [o], A. Atamanchuk [ℓ], T. Azemoon [p], T. Aziz [q,r], P.V.K.S. Baba [i], P. Bagnaia [s], J.A. Bakken [t], L. Baksay [u], R.C. Ball [p], S. Banerjee [q], J. Bao [d], R. Barillère [e], L. Barone [s], R. Battiston [h], A. Bay [v], F. Becattini [a], U. Becker [k,j], F. Behner [j], J. Behrens [j], S. Beingessner [w], Gy.L. Bencze [x], J. Berdugo [b], P. Berges [k], B. Bertucci [h], B.L. Betev [m,j], M. Biasini [h], A. Biland [j], G.M. Bilei [h], R. Bizzarri [s], J.J. Blaising [w], B. Blumenfeld [d], G.J. Bobbink [c,y], M. Bocciolini [a], R. Bock [r], A. Böhm [r], B. Borgia [s], D. Bourilkov [z], M. Bourquin [v], D. Boutigny [w], B. Bouwens [y], E. Brambilla [f], J.G. Branson [aa], I.C. Brock [ab], M. Brooks [ac], C. Buisson [ad], A. Bujak [ae], J.D. Burger [k], W.J. Burger [v], J.P. Burq [ad], J. Busenitz [u], X.D. Cai [i], M. Capell [af], M. Caria [h], F. Carminati [a], A.M. Cartacci [a], M. Cerrada [b], F. Cesaroni [s], Y.H. Chang [k], U.K. Chaturvedi [i], M. Chemarin [ad], A. Chen [ag], C. Chen [ah], G.M. Chen [ah], H.F. Chen [ai], H.S. Chen [ah], J. Chen [k], M. Chen [k], M.L. Chen [p], W.Y. Chen [i], G. Chiefari [f], C.Y. Chien [d], M. Chmeissani [p], S. Chung [k], C. Civinini [a], I. Clare [k], R. Clare [k], T.E. Coan [ac], H.O. Cohn [aj], G. Coignet [w], N. Colino [e], A. Contin [n], F. Crijns [z], X.T. Cui [i], X.Y. Cui [i], T.S. Dai [k], R. D'Alessandro [a], R. de Asmundis [f], A. Degré [w], K. Deiters [k], E. Dénes [x], P. Denes [t], F. DeNotaristefani [s], M. Dhina [j], D. DiBitonto [u], M. Diemoz [s], H.R. Dimitrov [m], C. Dionisi [s,e], M.T. Dova [i], E. Drago [f], T. Driever [z], D. Duchesneau [v], P. Duinker [y], H. El Mamouni [ad], A. Engler [ab], F.J. Eppling [k], F.C. Erné [y], P. Extermann [v], R. Fabbretti [ak], M. Fabre [ak], S. Falciano [s], S.J. Fan [aℓ], O. Fackler [af], J. Fay [ad], M. Felcini [e], T. Ferguson [ab], D. Fernandez [b], G. Fernandez [b], F. Ferroni [s], H. Fesefeldt [r], E. Fiandrini [h], J. Field [v], F. Filthaut [z], G. Finocchiaro [s], P.H. Fisher [d], G. Forconi [v], T. Foreman [y], K. Freudenreich [j], W. Friebel [am], M. Fukushima [k], M. Gailloud [an], Yu. Galaktionov [o,k], E. Gallo [a], S.N. Ganguli [q], P. Garcia-Abia [b], S.S. Gau [ag], D. Gele [ad], S. Gentile [s,e], S. Goldfarb [p], Z.F. Gong [ai], E. Gonzalez [b], P. Göttlicher [r], A. Gougas [d], D. Goujon [v], G. Gratta [ao], C. Grinnell [k], M. Gruenewald [ao], C. Gu [i], M. Guanziroli [i], J.K. Guo [aℓ], V.K. Gupta [t], A. Gurtu [e,q], H.R. Gustafson [p], L.J. Gutay [ae], K. Hangarter [r], A. Hasan [i], D. Hauschildt [y], C.F. He [aℓ], T. Hebbeker [r], M. Hebert [aa], G. Herten [k], U. Herten [r], A. Hervé [e], K. Hilgers [r], H. Hofer [j], H. Hoorani [v], G. Hu [i], G.Q. Hu [aℓ], B. Ille [ad], M.M. Ilyas [i], V. Innocente [e,f], H. Janssen [e], S. Jezequel [w], B.N. Jin [ah], L.W. Jones [p], A. Kasser [an], R.A. Khan [i], Yu. Kamyshkov [aj], P. Kapinos [ℓ], J.S. Kapustinsky [ac], Y. Karyotakis [e,w], M. Kaur [i], S. Khokhar [i], M.N. Kienzle-Focacci [v], W.W. Kinnison [ac], D. Kirkby [ao], S. Kirsch [am], W. Kittel [z], A. Klimentov [k,o], A.C. König [z], E. Koffeman [y], O. Kornadt [r], V. Koutsenko [k,o], A. Koulbardis [ℓ], R.W. Kraemer [ab], T. Kramer [k], V.R. Krastev [m,h], W. Krenz [r], A. Krivshich [ℓ], K.S. Kumar [ap], A. Kunin [ap,o], G. Landi [a], D. Lanske [r], S. Lanzano [f], P. Lebrun [ad], P. Lecomte [j], P. Lecoq [e], P. Le Coultre [j], D.M. Lee [ac], I. Leedom [g], J.M. Le Goff [e], R. Leiste [am], M. Lenti [a], E. Leonardi [s], J. Lettry [j], X. Leytens [y], C. Li [ai,i], H.T. Li [ah], P.J. Li [aℓ], X.G. Li [ah], J.Y. Liao [aℓ], W.T. Lin [ag], Z.Y. Lin [ai], F.L. Linde [e,y], B. Lindemann [r], D. Linnhofer [j], Y. Liu [i], W. Lohmann [am,e],

E. Longo [s], Y.S. Lu [ah], J.M. Lubbers [e], K. Lübelsmeyer [r], C. Luci [s], D. Luckey [n,k], L. Ludovici [s], L. Luminari [s], W.G. Ma [ai], M. MacDermott [j], P.K. Malhotra [q,l], R. Malik [i], A. Malinin [w,o], C. Maña [b], D.N. Mao [p], Y.F. Mao [ah], M. Maolinbay [j], P. Marchesini [j], F. Marion [w], A. Marin [c], J.P. Martin [ad], L. Martinez-Laso [e], F. Marzano [s], G.G.G. Massaro [y], T. Matsuda [k], K. Mazumdar [q], P. McBride [ap], T. McMahon [ae], D. McNally [j], Th. Meinholz [r], M. Merk [z], L. Merola [f], M. Meschini [a], W.J. Metzger [z], Y. Mi [i], G.B. Mills [ac], Y. Mir [i], G. Mirabelli [s], J. Mnich [r], M. Möller [r], B. Monteleoni [a], R. Morand [w], S. Morganti [s], N.E. Moulai [i], R. Mount [ao], S. Müller [r], A. Nadtochy [ℓ], E. Nagy [x], M. Napolitano [f], H. Newman [ao], C. Neyer [j], M.A. Niaz [i], A. Nippe [r], H. Nowak [am], G. Organtini [s], D. Pandoulas [r], S. Paoletti [a], G. Passaleva [a,h], S. Patricelli [f], T. Paul [d], M. Pauluzzi [h], F. Pauss [j], Y.J. Pei [r], D. Perret-Gallix [w], J. Perrier [v], A. Pevsner [d], M. Pieri [e,a], P.A. Piroué [t], F. Plasil [aj], V. Plyaskin [o], M. Pohl [j], V. Pojidaev [o,a], N. Produit [v], J.M. Qian [p], K.N. Qureshi [i], R. Raghavan [q], G. Rahal-Callot [j], G. Raven [y], P. Razis [aq], K. Read [aj], D. Ren [j], Z. Ren [i], M. Rescigno [s], S. Reucroft [g], A. Ricker [r], S. Riemann [am], O. Rind [p], H.A. Rizvi [i], B.P. Roe [p], M. Röhner [r], S. Röhner [r], L. Romero [b], J. Rose [r], S. Rosier-Lees [w], R. Rosmalen [z], Ph. Rosselet [an], A. Rubbia [k], J.A. Rubio [e,b], H. Rykaczewski [j], M. Sachwitz [am], E. Sajan [h], J. Salicio [e,b], J.M. Salicio [b], G.S. Sanders [ac], A. Santocchia [h], M.S. Sarakinos [k], G. Sartorelli [n,i], M. Sassowsky [r], G. Sauvage [w], V. Schegelsky [ℓ], K. Schmiemann [r], D. Schmitz [r], P. Schmitz [r], M. Schneegans [w], H. Schopper [ar], D.J. Schotanus [z], S. Shotkin [k], H.J. Schreiber [am], J. Shukla [ab], R. Schulte [r], S. Schulte [r], K. Schultze [r], J. Schütte [ap], J. Schwenke [r], G. Schwering [r], C. Sciacca [f], I. Scott [ap], R. Sehgal [i], P.G. Seiler [ak], J.C. Sens [e,y], L. Servoli [h], I. Sheer [aa], D.Z. Shen [aℓ], S. Shevchenko [ao], X.R. Shi [ao], E. Shumilov [o], V. Shoutko [o], E. Soderstrom [t], A. Sopczak [aa], C. Spartiotis [d], T. Spickermann [r], P. Spillantini [a], R. Starosta [r], M. Steuer [n,k], D.P. Stickland [t], F. Sticozzi [k], H. Stone [v], K. Strauch [ap], B.C. Stringfellow [ae], K. Sudhakar [q,r], G. Sultanov [i], R.L. Sumner [t], L.Z. Sun [ai,i], H. Suter [j], R.B. Sutton [ab], J.D. Swain [i], A.A. Syed [i], X.W. Tang [ah], L. Taylor [g], C. Timmermans [z], Samuel C.C. Ting [k], S.M. Ting [k], M. Tonutti [r], S.C. Tonwar [q], J. Tóth [x], A. Tsaregorodtsev [ℓ], G. Tsipolitis [ab], C. Tully [ao], K.L. Tung [ah], J. Ulbricht [j], L. Urbán [x], U. Uwer [r], E. Valente [s], R.T. Van de Walle [z], I. Vetlitsky [o], G. Viertel [j], P. Vikas [i], U. Vikas [i], M. Vivargent [w], H. Vogel [ab], H. Vogt [am], I. Vorobiev [o], A.A. Vorobyov [ℓ], L. Vuilleumier [an], M. Wadhwa [i], W. Wallraff [r], C.R. Wang [ai], G.H. Wang [ab], J.H. Wang [ah], Q.F. Wang [ap], X.L. Wang [ai], Y.F. Wang [a], Z.M. Wang [i,ai], A. Weber [r], J. Weber [j], R. Weill [an], T.J. Wenaus [af], J. Wenninger [v], M. White [k], C. Willmott [b], F. Wittgenstein [e], D. Wright [t], R.J. Wu [ah], S.X. Wu [i], Y.G. Wu [ah], B. Wysłouch [k], Y.Y. Xie [aℓ], Y.D. Xu [ah], Z.Z. Xu [ai], Z.L. Xue [aℓ], D.S. Yan [aℓ], X.J. Yan [k], B.Z. Yang [ai], C.G. Yang [ah], G. Yang [i], K.S. Yang [ah], Q.Y. Yang [ah], Z.Q. Yang [aℓ], C.H. Ye [i], J.B. Ye [ai], Q. Ye [i], S.C. Yeh [ag], Z.W. Yin [aℓ], J.M. You [i], N. Yunus [i], M. Yzerman [y], C. Zaccardelli [ao], P. Zemp [j], M. Zeng [i], Y. Zeng [r], D.H. Zhang [y], Z.P. Zhang [ai,i], B. Zhou [c], J.F. Zhou [r], R.Y. Zhu [ao], H.L. Zhuang [ah], A. Zichichi [n,e,i] and B.C.C. van der Zwaan [y]

[a] *INFN – Sezione di Firenze and Università di Firenze, I-50125 Florence, Italy*
[b] *Centro de Investigaciones Energeticas, Medioambientales y Tecnologicas, CIEMAT, E-28040 Madrid, Spain*
[c] *Boston University, Boston, MA 02215, USA*
[d] *Johns Hopkins University, Baltimore, MD 21218, USA*
[e] *European Laboratory for Particle Physics, CERN, CH-1211 Geneva 23, Switzerland*
[f] *INFN – Sezione di Napoli and Università di Napoli, I-80125 Naples, Italy*
[g] *Northeastern University, Boston, MA 02115, USA*
[h] *INFN – Sezione di Perugia and Università Degli Studi di Perugia, I-06100 Perugia, Italy*
[i] *World Laboratory, FBLJA Project, CH-1211 Geneva, Switzerland*
[j] *Eidgenössische Technische Hochschule, ETH Zürich, CH-8093 Zurich, Switzerland*
[k] *Massachusetts Institute of Technology, Cambridge, MA 02139, USA*

[f] *Nuclear Physics Institute, 188 350 St. Petersburg, Russian Federation*
[m] *Bulgarian Academy of Sciences, Institute of Mechatronics, BU-1113 Sofia, Bulgaria*
[n] *INFN – Sezione di Bologna, I-40126 Bologna, Italy*
[o] *Institute of Theoretical and Experimental Physics, ITEP, 117 259 Moscow, Russian Federation*
[p] *University of Michigan, Ann Arbor, MI 48109, USA*
[q] *Tata Institute of Fundamental Research, Bombay 400 005, India*
[r] *I. Physikalisches Institut, RWTH, W-5100 Aachen, FRG*[2]
and III. Physikalisches Institut, RWTH, W-5100 Aachen, FRG[2]
[s] *INFN – Sezione di Roma and Università di Roma "La Sapienza", I-00185 Rome, Italy*
[t] *Princeton University, Princeton, NJ 08544, USA*
[u] *University of Alabama, Tuscaloosa, AL 35486, USA*
[v] *University of Geneva, CH-1211 Geneva 4, Switzerland*
[w] *Laboratoire de Physique des Particules, LAPP, F-74519 Annecy-le-Vieux, France*
[x] *Central Research Institute for Physics of the Hungarian Academy of Sciences, H-1525 Budapest 114, Hungary*
[y] *National Institute for High Energy Physics, NIKHEF, NL-1009 DB Amsterdam, The Netherlands*
[z] *University of Nijmegen and NIKHEF, NL-6525 ED Nijmegen, The Netherlands*
[aa] *University of California, San Diego, CA 92182, USA*
[ab] *Carnegie Mellon University, Pittsburgh, PA 15213, USA*
[ac] *Los Alamos National Laboratory, Los Alamos, NM 87544, USA*
[ad] *Institut de Physique Nucléaire de Lyon, IN2P3-CNRS/Université Claude Bernard, F-69622 Villeurbanne Cedex, France*
[ae] *Purdue University, West Lafayette, IN 47907, USA*
[af] *Lawrence Livermore National Laboratory, Livermore, CA 94550, USA*
[ag] *High Energy Physics Group, Taiwan, ROC*
[ah] *Institute of High Energy Physics, IHEP, Beijing, China*
[ai] *Chinese University of Science and Technology, USTC, Hefei, Anhui 230 029, China*
[aj] *Oak Ridge National Laboratory, Oak Ridge, TN 37830, USA*
[ak] *Paul Scherrer Institut, PSI, CH-5232 Villigen, Switzerland*
[af] *Shanghai Institute of Ceramics, SIC, Shanghai, China*
[am] *Institut für Hochenergiephysik, O-1615 Zeuthen–Berlin, FRG*[2]
[an] *University of Lausanne, CH-1015 Lausanne, Switzerland*
[ao] *California Institute of Technology, Pasadena, CA 91125, USA*
[ap] *Harvard University, Cambridge, MA 02139, USA*
[aq] *Department of Natural Sciences, University of Cyprus, Nicosia, Cyprus*
[ar] *University of Hamburg, W-2000 Hamburg, FRG*

Received 18 May 1992

We present a study of the inclusive η production based on 300 000 hadronic Z^0 decays. The measured inclusive momentum distribution can be reproduced by parton shower Monte Carlo programs and also by an analytical QCD calculation. Comparing our results with low energy e^+e^- data, we find that QCD describes both the shape and the energy evolution of the η spectrum. The comparison of η production rates in quark- and gluon-enriched jet samples does not show statistically significant evidence for more abundant production of η mesons in gluon fragmentation.

1. Introduction

We report here on a measurement of inclusive η production at the Z^0 resonance using the L3 detector at LEP. The η mesons are identified through their

[1] Deceased.
[2] Supported by the German Bundesministerium für Forschung und Technologie.

two-photon decays, measured by the electromagnetic calorimeter.

Hadron production in Z^0 decays proceeds through two main steps: parton shower development from the primary $q\bar{q}$ pair produced from the Z^0, followed by fragmentation of the coloured partons into colourless hadrons. Measurement of inclusive η production is particularly suited for studies of e^+e^- hadroproduction, since most of the η mesons are direct fragmentation products rather than stemming from decays of other particles.

The measured inclusive η meson momentum spectrum is compared with the predictions of the Monte Carlo generators JETSET 7.3 [1] and HERWIG 5.4 [2]. Both programs implement a parton cascade based on perturbative QCD calculations, whereas the non-perturbative hadronization phase is described by a specific phenomenological model – the string and the cluster fragmentation models, respectively.

We also compare the measured spectrum with the analytical calculations performed in the framework of the "modified leading log approximation" (MLLA) of QCD [3], in which single and double leading log contributions are taken into account and coherence effects are included. Complemented with the "local parton hadron duality" assumption [3,4], where the non-perturbative effects are reduced to normalizing constants relating hadronic characteristics to partonic ones, the calculated MLLA inclusive parton spectrum can be directly compared with the measured hadron spectrum.

Finally, the study of η production provides a means to test the theoretical expectations for enhanced production of isoscalar mesons in gluon jets [5]. To this end, we present a comparison of the η production rates in quark- and gluon-enriched jet samples.

2. The L3 detector

The L3 detector has previously been described in detail in ref. [6]. It consists of a central tracking chamber, a high resolution electromagnetic calorimeter composed of bismuth germanium oxide crystals, a ring of scintillation counters, a uranium and brass hadron calorimeter with proportional wire chamber readout, and an accurate muon chamber system. These detectors are installed in a 12 m diameter magnet which provides a uniform field of 0.5 T along the beam direction.

The central tracking chamber (TEC) is a time expansion chamber which consists of two cylindrical layers of 12 and 24 sectors, with 62 sense wires measuring the R–ϕ coordinate. The single wire resolution is 58 μm averaged over the entire cell.

The material preceding the barrel part of the electromagnetic detector amounts to less than 10% of a radiation length. In that region the energy resolution is 5% for photons and electrons of energy around 100 MeV, and is less than 2% for energies above 1.5 GeV. The angular resolution of electromagnetic clusters is better than 0.5° for energies above 1 GeV.

For the present analysis, we use the data collected in the following ranges of polar angles:
- for the central tracking chamber, $40° < \theta < 140°$,
- for the electromagnetic calorimeter, $11° < \theta < 169°$,
- for the hadron calorimeter, $5° < \theta < 175°$.

3. Event selection

Events collected at center of mass energies around $\sqrt{s} = 91.2$ GeV ($88.4 \leqslant \sqrt{s} \leqslant 93.7$ GeV) from the 1991 LEP running period are used for this analysis.

The selection of events of the type $e^+e^- \rightarrow$ hadrons is based on the energy measured in the electromagnetic detector and in the hadron calorimeter. Events are accepted if:
- $N_{\text{cluster}} > 15$,
- $0.5 < E_{\text{vis}}/\sqrt{s} < 1.5$,
- $|E_{\parallel}|/E_{\text{vis}} < 0.5$, $E_{\perp}/E_{\text{vis}} < 0.5$,

where E_{vis} is the total energy observed in the calorimeters, $E_{\parallel}$ is the energy imbalance along the beam direction, $E_{\perp}$ is the energy imbalance in the plane perpendicular to the beam direction, and N_{cluster} is the number of calorimetric clusters with energy greater than 100 MeV. After excluding the runs with bad beam background conditions, 297 300 events passed the selection cuts.

We used two sets of 500 000 and 300 000 Monte Carlo events generated by the parton shower programs JETSET 7.3 [1] and HERWIG 5.4 [2], respectively. The values for the QCD scale and the fragmentation parameters were determined from fits to our data [7]. The generated events were passed through the L3 de-

tector simulation [8], which implements a detailed description of the L3 detector and takes into account the effects of energy loss, multiple scattering, interactions and decays in the detector materials and the beam pipe. These events were processed with the same reconstruction and analysis programs as the experimental data.

Applying the same selection of hadronic Z^0 decays to the simulated events as for the data, we find that 98% of the hadronic decays from the Z^0 are accepted. The contamination from final states e^+e^-, $\tau^+\tau^-$ and hadronic production via two-photon processes is estimated to be less than 0.2% and is neglected.

4. Photon selection

The η mesons are detected through their two-photon decay mode as a narrow peak in the $\gamma\gamma$ invariant mass distribution.

Photons are recognized as isolated and confined clusters in the electromagnetic calorimeter, a cluster being a matrix of 3×3 crystals centered on the most energetic crystal. An electromagnetic cluster is considered as a photon candidate if it is not matched within a momentum-dependent angular window of 20–35 mrad with any extrapolated charged track trajectory, measured in the central tracking chamber.

The photon energy is calculated from the energy of the cluster by applying a position-dependent leakage correction. Assuming that the photon originates at the e^+e^- interaction point, its direction is determined from the geometrical positions of the constituent crystals, weighted by the corresponding energy deposits. The photons used in the η analysis are required to satisfy the following cuts:

(1) $E_\gamma > 500$ MeV,
(2) $44.5° < \theta_\gamma < 135.5°$,
(3) $E_\gamma/E_{25} > 0.90$,
(4) $E_{\mathrm{had}}/E_\gamma < 0.10$,

where E_γ denotes the energy and θ_γ the polar angle of the photon. E_{25} is the leakage corrected energy deposited in the 5×5 symmetric extension of the 3×3 crystal array. E_{had} stands for the energy deposited in the six innermost hadron calorimeter layers inside a cone with half opening angle of 100 mrad around the photon direction.

By imposing cut (2) photons are accepted only if they are detected in the barrel part of the electromagnetic calorimeter. The isolation cuts (3) and (4) reject background from hadrons. Additional suppression of hadron-shower debris faking electromagnetic clusters is achieved by requiring the lateral energy deposition pattern to be consistent with that of an electromagnetic shower, as determined from test beam data.

The finite granularity of the electromagnetic calorimeter sets a lower bound of $\sim 6°$ on the opening angle of detected pairs of photons, which effectively limits the energy of the observed η mesons decaying into non-overlapping photons to below about 10 GeV.

5. Inclusive η production spectrum

The $\gamma\gamma$ invariant mass spectrum is measured using photon pairs in which both photons are in the same hemisphere defined by a plane perpendicular to the event thrust axis. Most of the photons observed in a hadronic Z^0 decay originate from π^0 mesons decaying into two photons, the average π^0 multiplicity being close to 10 [9]. To reduce the combinatorial background related to π^0 decays, we apply the π^0 selection procedure as described in ref. [9], and exclude from the η analysis all photons entering into a two-photon combination with invariant mass compatible with the π^0 mass within 3σ, the observed π^0 signal having a width of $\sigma = 7$ MeV.

Fig. 1 shows the resulting $\gamma\gamma$ invariant mass distribution in the kinematic region $0.035 < x_p < 0.225$, where $x_p = p/E_{\mathrm{beam}}$ denotes the ratio of the η momentum to the beam energy. The fit to the mass distribution, indicated by a solid line, is a sum of a gaussian function and a third order polynomial. The η peak is centered at 548.3 ± 0.6 MeV, has a width of $\sigma = 16.1 \pm 0.6$ MeV and contains 1848 ± 80 η mesons. The observed resolution is consistent with the Monte Carlo expectation.

To determine the x_p distribution of reconstructed η mesons, the measurement of the invariant mass distribution and the fit were repeated for different x_p intervals. The η yield as a function of the variable $\xi_p = \ln(1/x_p)$ was obtained in a similar way.

To calculate the differential cross sections, the observed yields of η mesons in the data have been corrected, bin by bin, for detector effects (acceptance, ef-

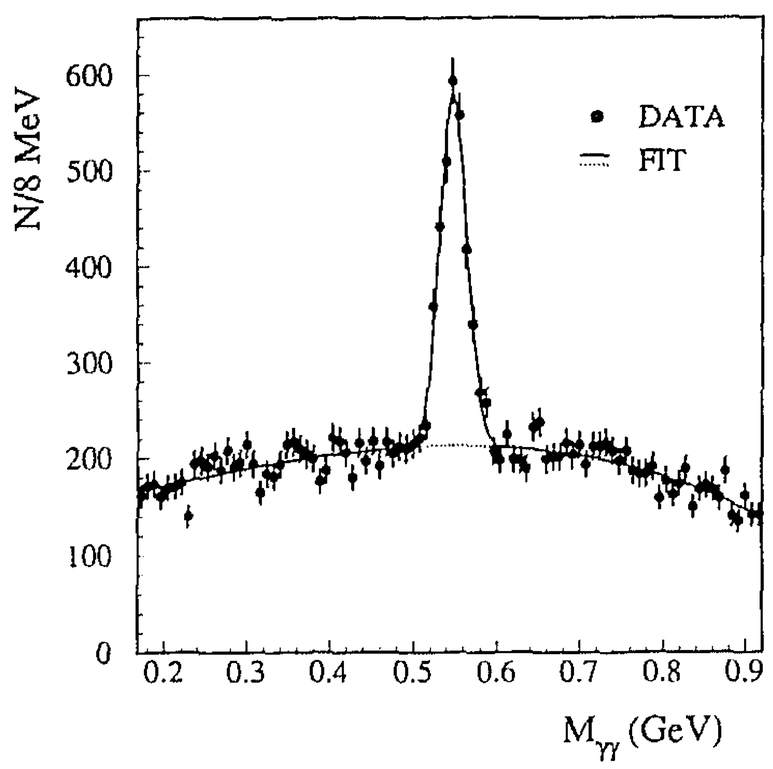

Fig. 1. Measured two-photon invariant mass distribution. The solid line represents the result of a fit to the data using a sum of a gaussian distribution and a third order polynomial. The dotted line indicates the background. The η signal has a width of $\sigma = 16.1 \pm 0.6$ MeV.

ficiency and resolution). The detector correction factors were calculated using the JETSET Monte Carlo events that were passed through the detector simulation and reconstruction programs. The η detection efficiencies, including the 38.9% branching ratio of the η meson into two photons, were found to be of the order of 1%. The JETSET program was also used to compute the correction factors for initial state photon radiation, which on average are equal to unity within 1%.

Systematic uncertainties in the calculated η differential cross sections were estimated by varying the η selection cuts, varying the selection of TEC tracks used for veto, and switching off the π^0 background suppression procedure. The order of the polynomial used to describe the background in the invariant mass fit was varied, as well as the mass range of the fits. In addition, in order to study the effect of fragmentation uncertainties, we have calculated the η differential cross sections with the acceptance derived from the HERWIG Monte Carlo event sample. The different contributions to the systematic errors, of which the fragmentation uncertainty is the dominant one, were added in quadrature. The resulting systematic errors are in the range (12–18)% and are of the same order as the statistical ones.

The differential cross sections for inclusive η production at the Z^0 resonance, normalized to the total hadronic cross section σ_h, are given in table 1 and shown in figs. 2 and 3 as a function of the variables x_p and ξ_p, respectively.

6. Comparison to QCD predictions

In fig. 2 the measured differential cross section

$$(1/\sigma_h)\, d\sigma/dx_p$$

for η mesons is compared to the predictions of the parton shower Monte Carlo programs JETSET and HERWIG. The QCD scale and fragmentation parameters used in the Monte Carlo programs are determined from a comparison to the hadronic event shape distributions calculated from L3 data [7]. Within the errors, the measured η meson production is in agreement with both Monte Carlo models.

We also compare the measured inclusive η spectrum with the MLLA QCD calculations, following the same method we have applied in the analysis of our π^0 and

Table 1
Differential cross sections for inclusive η production, normalized to the total hadronic cross section. The first errors are statistical, the second are the systematic ones.

x_p	$(1/\sigma_h)\, d\sigma/dx_p$	ξ_p	$(1/\sigma_h)\, d\sigma/d\xi_p$
0.035–0.045	$9.19 \pm 1.38 \pm 1.10$	1.4–1.8	$0.262 \pm 0.045 \pm 0.047$
0.045–0.065	$6.48 \pm 0.77 \pm 0.97$	1.8–2.1	$0.406 \pm 0.055 \pm 0.069$
0.065–0.095	$5.20 \pm 0.58 \pm 0.83$	2.1–2.4	$0.378 \pm 0.047 \pm 0.060$
0.095–0.135	$3.30 \pm 0.42 \pm 0.53$	2.4–2.7	$0.408 \pm 0.052 \pm 0.065$
0.135–0.175	$2.61 \pm 0.38 \pm 0.42$	2.7–3.0	$0.361 \pm 0.047 \pm 0.054$
0.175–0.225	$1.26 \pm 0.23 \pm 0.23$	3.0–3.2	$0.384 \pm 0.061 \pm 0.050$
		3.2–3.4	$0.310 \pm 0.060 \pm 0.040$

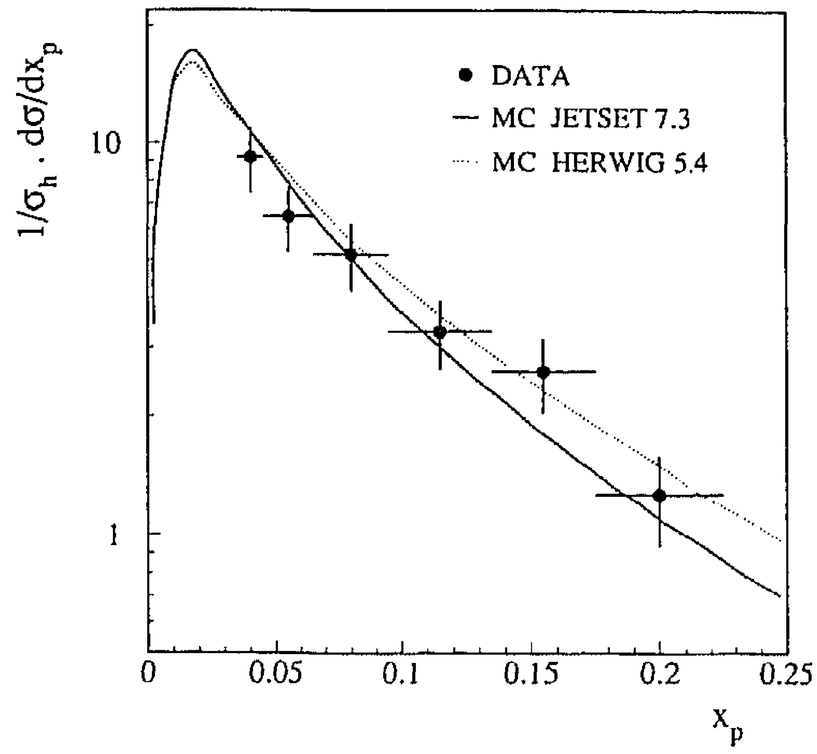

Fig. 2. The x_p spectrum for inclusive η production at the Z^0 resonance normalized to the total hadronic cross section in comparison with the predictions of Monte Carlo parton shower generators. The errors (vertical bars) include statistical and systematic uncertainties added in quadrature. The horizontal bars indicate the bin size.

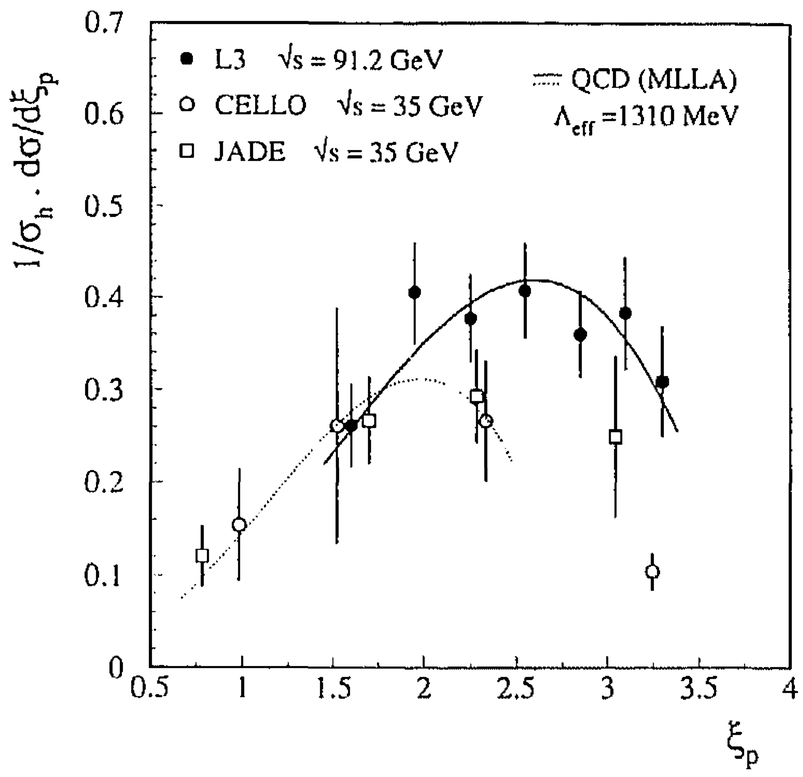

Fig. 3. Inclusive ξ_p spectrum normalized to the total hadronic cross section in comparison with the analytical QCD calculations. Besides the L3 spectrum, results from the CELLO and JADE Collaborations are also shown. The errors are only statistical. The value of $\Lambda_{\rm eff}$ used in the QCD calculation is determined from a fit to the L3 data.

charged particle spectra in ref. [9]. We use the MLLA expression for the so-called *limiting spectrum*, which is convenient for numerical integration and can be written in the form

$$\frac{1}{\sigma_{\rm h}}\frac{{\rm d}\sigma}{{\rm d}\xi_p} = N(\sqrt{s})\, f(\sqrt{s}, \Lambda_{\rm eff}; \xi_p)\,. \qquad (1)$$

There are only two free parameters in eq. (1): an overall normalization factor N, which describes the hadronization and depends on the center of mass energy $\sqrt{s}$ and on the particle type, and an effective scale parameter $\Lambda_{\rm eff}$ (not directly related to $\Lambda_{\overline{\rm MS}}$). Formula (1) is valid in the range $1 < \xi_p < \ln(0.5\sqrt{s}/\Lambda_{\rm eff})$.

Expression (1) for the limiting inclusive spectrum embodies two distinct features: the existence of a maximum in the ξ_p distribution and a prediction of the energy evolution of the position of the maximum. These features, already observed in the analysis of our π^0 and charged particle data samples [9], are also present in the η data. This is illustrated in fig. 3, which shows our measured η differential cross section $(1/\sigma_{\rm h})\,{\rm d}\sigma/{\rm d}\xi_p$, as well as spectra measured at a lower center of mass energy [10,11]. We fit expression (1) to our data and obtain

$$N = 0.138 \pm 0.011 \pm 0.031\,,$$

$$\Lambda_{\rm eff} = 1310 \pm 175 \pm 200\,{\rm MeV}\,,$$

$$\xi_p^* = 2.60 \pm 0.10 \pm 0.11\,,$$

where ξ_p^* denotes the position of the maximum corresponding to the measured $\Lambda_{\rm eff}$. The first error on each parameter is statistical and the second one is systematic. The systematic errors have been determined from the differences of the fits to the cross section sets used to evaluate the systematic uncertainties of the measured inclusive η spectrum. The QCD prediction for $\sqrt{s} = 91$ GeV based on the fitted parameters is shown in fig. 3 as a solid line.

The limiting spectrum (1), evaluated at a center of mass energy of 35 GeV using our measured value for $\Lambda_{\rm eff}$, is valid in the region of $\xi_p < 2.6$. The QCD prediction for the data taken at $\sqrt{s} = 35$ GeV is obtained from a combined fit to the data sets from refs. [10,11], using the same value of $\Lambda_{\rm eff}$ as determined from our data at $\sqrt{s} = 91$ GeV, and with the normalization factor N as the only free parameter. The MLLA calculation, shown in fig. 3 as a dotted line, reproduces well these measurements.

We also fit the MLLA function (1) to each 35 GeV data set separately in the region around their maxima, leaving the parameters $\Lambda_{\rm eff}$ and N free. The corresponding peak positions ξ_p^* for the η spectra are shown in fig. 4, together with the peak positions for the π^0 spectra, as determined in ref. [9] where lower

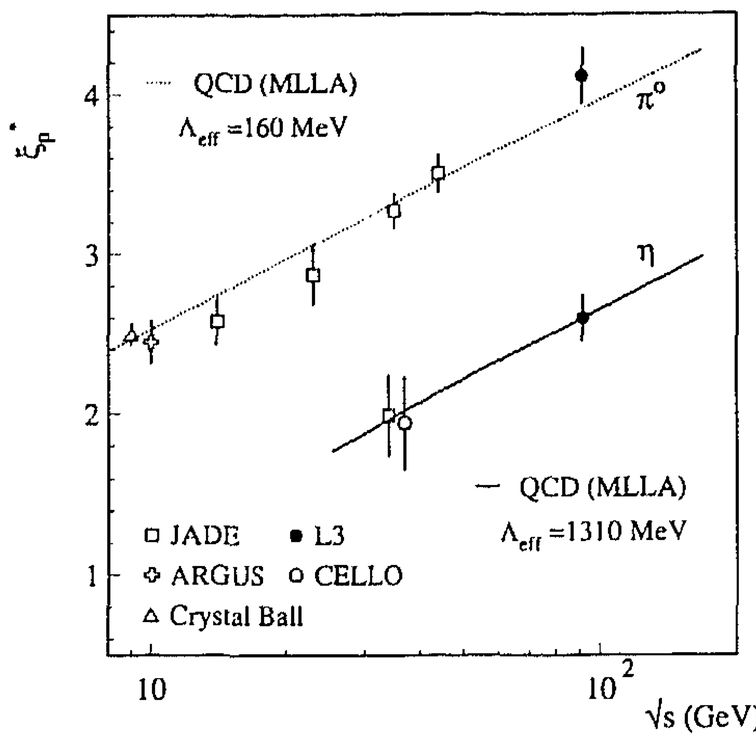

Fig. 4. Energy dependence of the position of the maximum, ξ_p^*, in the ξ_p distributions for neutral pions and η mesons. The lines represent the QCD predictions. Different points at the same center of mass energy are shifted horizontally.

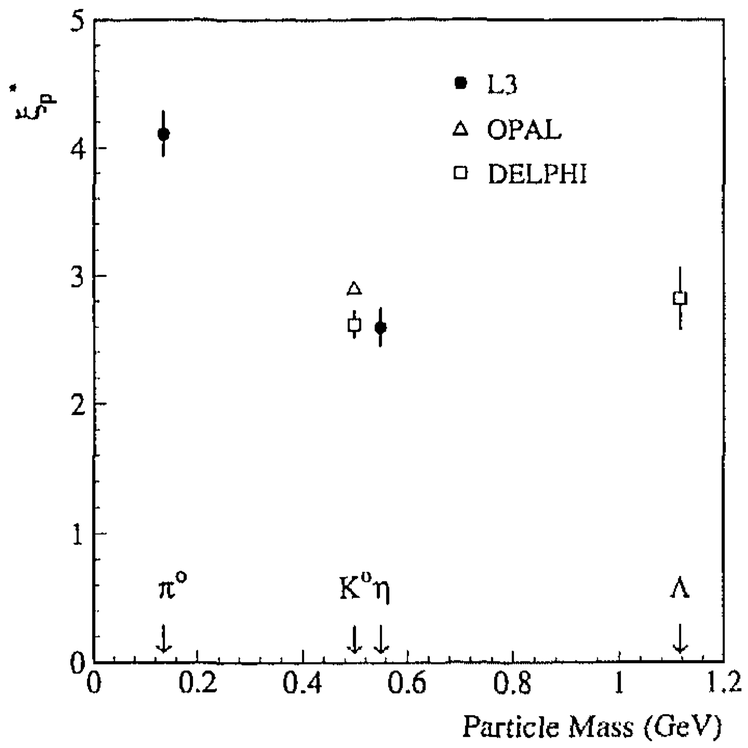

Fig. 5. Position of the maximum, ξ_p^*, in the measured ξ_p distributions for identified particles at $\sqrt{s} = 91$ GeV, versus particle mass.

energy π^0 data from refs. [10,12,13] have also been included. The energy evolution of the peak positions is consistent with the QCD formula (1). The observed shift of the peak position towards lower ξ_p values with increasing particle mass is also expected by MLLA, although no specific prediction exists for it. In fig. 5 we plot the position of the maximum ξ_p^* versus particle mass for identified particle spectra measured at LEP [9,14]. The peak position of the K^0 spectrum is close to that of the η, both particles having similar masses.

7. Production rates of η mesons in multi-jet events

We have studied η production in quark- and gluon-induced jets by comparing the production rates observed in the data with the corresponding rates in the Monte Carlo event samples. Neither the JETSET nor HERWIG Monte Carlo generators implement any mechanism for enhanced isoscalar meson production in gluon fragmentation.

In the present analysis, jets in an event are identified with the LUCLUS jet finding algorithm [15], which is based on an unscaled resolution parameter d_{join}, measured in GeV. The LUCLUS jet finder combines two particles into a cluster if the transverse momentum of either particle with respect to the vector sum of their momenta does not exceed the d_{join} value. To reject spurious jets, we require the energy E_{jet} and the number of the constituent calorimetric clusters N_{con} of the reconstructed jets to satisfy the following cuts:

- $E_{jet} > 5$ GeV,
- $N_{con} \geqslant 4$.

In order to calculate the production yields of η mesons in quark- and gluon-enriched jet samples, we select events with three or more jets. For a cutoff parameter value $d_{join} = 4$ GeV, 52% of the hadronic events have a jet multiplicity greater than two. Such events are used to calculate two $\gamma\gamma$ invariant mass distributions: one using photon pairs for which the nearest jet to the pair is the most energetic or the second most energetic jet in the event, and another invariant mass spectrum calculated with photon pairs for which the nearest jet has an energy lower than the second most energetic jet. From a Monte Carlo study of the nearest jets to photon pairs having invariant mass close to the η mass, we estimate that for $d_{join} = 4$ GeV the jet sample comprising the most energetic and the second most energetic jets has 75% quark jet purity, and the lower energy jet sample has 78% gluon jet purity. In the Monte Carlo study we have considered a jet, reconstructed at the detector level, as a gluon jet, if the nearest jet, reconstructed at the parton level, did not contain a primary quark or antiquark from the Z^0 decay [#1]. By fitting the $\gamma\gamma$ invariant mass distributions, we evaluate the numbers of η mesons from the quark-enriched jet sample and

[#1] At the parton level, no cut on the energy and on the number of the jet constituents was imposed.

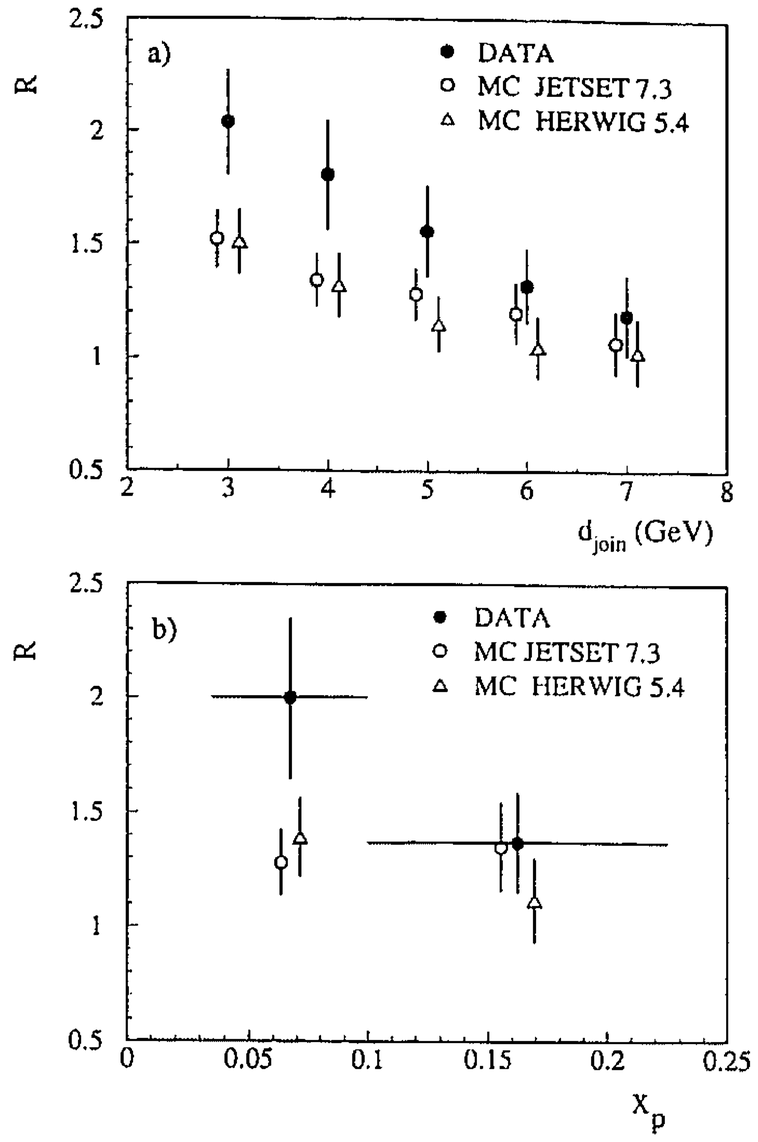

Fig. 6. Ratio of η yields in gluon- and quark-enriched jet samples observed in the data in comparison with Monte Carlo expectations (a) as a function of the d_{join} parameter and (b) as a function of x_p for $d_{join} = 4$ GeV. The errors (vertical bars) include statistical and systematic uncertainties added in quadrature. The horizontal bars of the data points in (b) indicate the bin size for the two groups of points. The Monte Carlo points are shifted horizontally with respect to the data points.

from the gluon-enriched jet sample respectively, and calculate the uncorrected ratio of the observed yields:

$$R = \frac{\#\ \text{of}\ \eta\ \text{mesons in lower energy jet sample}}{\#\ \text{of}\ \eta\ \text{mesons in higher energy jet sample}}.$$

The ratio R constructed in this way is sensitive to differences in production rates of η mesons in quark- and gluon-induced jets. We calculate this ratio for both data and Monte Carlo events and compare the results in fig. 6a, in which R is presented as a function of the jet resolution parameter d_{join}. The points shown in this plot are based on overlapping event samples and therefore are correlated. The statistical errors on the measured values of R are in the range of (10–12)% ((7–9)%) for the data (JETSET Monte Carlo) and the systematic uncertainties are of the order of (5–10)% ((4–9)%) for the data (Monte Carlo). With decreasing the d_{join} value the data show higher η production rates in the gluon-enriched jet sample than the Monte Carlo expectations. The observed deviations do not exceed 2σ and originate from differences in the rates in the low x_p region. This is illustrated by fig. 6b, which shows the ratio R calculated for $d_{join} = 4$ GeV in two x_p intervals.

At $\sqrt{s} = 35$ GeV, the JADE Collaboration has looked for differences of η production in gluon and quark fragmentation by comparing the yield of η mesons in planar and spherical events with the corresponding yield in two-jet events. The initial indication of higher η production rates in events with planar or spherical structure [16] was not supported by a later study based on increased statistics [13]. At lower center of mass energies, the ARGUS and Crystal Ball Collaborations have compared the η production rates measured in the direct decays of the $\Upsilon(1S)$ resonance with the rates in events from the nearby continuum [12]. No significant differences of η production rates in three gluon systems, resulting from the $\Upsilon(1S)$ decays, with respect to the η production rates in $q\bar{q}$ events from the continuum, have been observed.

The present analysis also does not provide statistically significant evidence for the enhanced production of η mesons in gluon fragmentation, predicted by the model in ref. [5].

8. Summary and conclusions

We have measured the production of η mesons from 300 000 hadronic Z^0 decays. The measured inclusive momentum distribution can be reproduced by both the parton shower Monte Carlo programs JETSET and HERWIG. We also observe that QCD analytical calculations provide a consistent way to describe the shape and the energy evolution of the η spectrum, and we measure an effective scale parameter value $\Lambda_{\text{eff}} = 1310 \pm 175 \pm 200$ MeV. The results of the study of η production rates in quark- and gluon-enriched jet samples do not show statistically significant evidence for more abundant production of η mesons in gluon fragmentation.

Acknowledgement

We wish to express our gratitude to the CERN accelerator divisions for the excellent performance of the LEP machine. In the course of the analysis we benefited from many discussions with T. Sjöstrand to whom we express our gratitude. We acknowledge the effort of all engineers and technicians who have participated in the construction and maintenance of this experiment.

References

[1] JETSET Monte Carlo program:
T. Sjöstrand, Comput. Phys. Commun. 39 (1986) 347;
T. Sjöstrand and M. Bengtsson, Comput. Phys. Commun. 43 (1987) 367.
[2] HERWIG Monte Carlo program:
G. Marchesini and B. Webber, Nucl. Phys. B 310 (1988) 461;
I.G. Knowles, Nucl. Phys. B 310 (1988) 571;
G. Marchesini et al., Comput. Phys. Commun. 67 (1992) 465.
[3] Y.L. Dokshitzer and S.I. Troyan, Leningrad preprint LNPI-922 (1984);
Y.I. Azimov et al., Z. Phys. C 27 (1985) 65; C 31 (1986) 213;
V.A. Khoze, Y.L. Dokshitzer and S.I. Troyan, Lund preprint LU TP 90-12.
[4] D. Amati and G. Veneziano, Phys. Lett. B 83 (1979) 87.
[5] C. Peterson and T.F. Walsh, Phys. Lett. B 91 (1980) 455.
[6] L3 Collab., B. Adeva et al., Nucl. Instrum. Methods A 289 (1990) 35.
[7] L3 Collab., B. Adeva et al., CERN preprint CERN-PPE/92-50.
[8] GEANT Version 3.14 (November 1990):
see R. Brun et al., "GEANT 3", CERN DD/EE/84-1 (Rev.) (September 1987).
[9] L3 Collab., B. Adeva et al., Phys. Lett. B 259 (1991) 199.
[10] JADE Collab., D.D. Pitzl et al., Z. Phys. C 46 (1990) 1.
[11] CELLO Collab., H.-J. Behrend et al., Z. Phys. C 47 (1990) 1.
[12] ARGUS Collab., H. Albrecht et al., Z. Phys. C 46 (1990) 15;
Crystal Ball Collab., C. Bieler et al., Z. Phys. C 49 (1990) 225.
[13] JADE Collab., W. Bartel et al., Z. Phys. C 28 (1985) 343.
[14] OPAL Collab., G. Alexander et al., Phys. Lett. B 264 (1991) 467;
DELPHI Collab., P. Abreu et al., Phys. Lett. B 275 (1992) 231.
[15] T. Sjöstrand, Comput. Phys. Commun. 28 (1983) 229.
[16] JADE Collab., W. Bartel et al., Phys. Lett. B 130 (1983) 454.